Layered Titanium Disilicide Stabilized by Oxide Coating for Highly Reversible Lithium Insertion and Extraction

Sa Zhou,[†] Zachary I. Simpson,[†] Xiaogang Yang, and Dunwei Wang*

Department of Chemistry, Merkert Chemistry Center, Boston College, 2609 Beacon Street, Chestnut Hill, Massachusetts 02467, United States.
[†]These authors contributed equally.

ABSTRACT

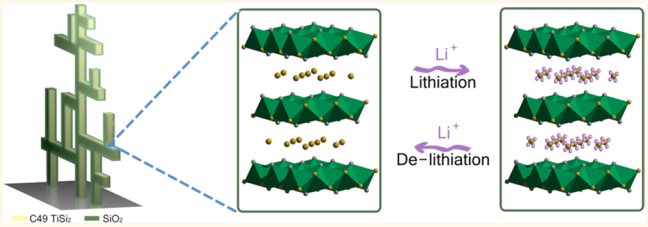

The discovery of new materials has played an important role in battery technology development. Among the newly discovered materials, those with layered structures are often of particular interest because many have been found to permit highly repeatable ionic insertion and extraction. Examples include graphite and $LiCoO_2$ as anode and cathode materials, respectively. Here we report C49 titanium disilicide ($TiSi_2$) as a new layered anode material, within which lithium ions can react with the Si-only layers. This result is enabled by the strategy of coating a thin (<5 nm) layer of oxide on the surface of $TiSi_2$. This coating helped us rule out the possibility that the measured capacity is due to surface reactions. It also stabilizes $TiSi_2$ to allow for the direct observation of $TiSi_2$ in its lithiated and delithiated states. In addition, this stabilization significantly improved the charge and discharge performance of $TiSi_2$. The confirmation that the lithium-ion storage capacity of $TiSi_2$ is a result of its layered structure is expected to have major fundamental and practical implications.

KEYWORDS: silicide · layered structures · lithium-ion battery · energy storage · electrode materials

With significant advantages such as long cycle lifetimes and relatively high specific capacities, the lithium-ion battery is a prevailing energy storage technology. Its development has benefited from the discovery of key new electrode materials, including graphite and $LiCO_2$ acting as an anode and a cathode, respectively.[1] These materials often exhibit a layered structure, which allows for Li^+ insertion and extraction with minimal influence on the host structure, thereby enabling long cycle lifetimes.[2] The measured specific capacities of these materials, however, are limited by their chemical nature and now fail to meet the ever-growing needs.[3] In comparison, high-capacity materials lacking a layered structure, such as Si,[4−7] Si-alloys,[8−10] Sn,[11,12] and SnO_2,[13,14] suffer from short cycle lifetimes due to structural degradations caused by Li^+ insertion and extraction. Finding new layered materials with high specific capacities should therefore be important in the development of lithium-ion battery technology. Herein we report that the $TiSi_2$ nanonet is such a material, with the combined benefits of a high specific capacity and a long cycle lifetime owing to the high content of Si and a layered crystal structure.

The key uniqueness of the $TiSi_2$ nanonet lies in its C49 crystal structure. As shown in Figure 1, the structure consists of flat Si-only layers separated by polyhedrons of Ti and Si. Since Si is known to alloy with Li, it is conceivable that the layered C49 structure can serve as an anode material. However, bulk C49 $TiSi_2$ has been demonstrated as metastable, transforming to a C54 structure upon heating.[15] The latter structure is still of orthorhombic symmetry but lacks the Si-only layers. As such, $TiSi_2$ has not demonstrated an appreciable capacity.[16] Previously, we discovered that the nanonet form of C49 $TiSi_2$ is stable up to 900 °C.[17] While the exact cause of the stabilization remains unknown, this new material serves as a platform to test the lithiation and delithiation properties of C49 $TiSi_2$. However, due to the reactions between Li^+ and Si, we have observed significant structural degradation of $TiSi_2$, leading to a loss of Ti into the electrolyte and the formation of amorphous Si on the nanonet surfaces.[18] In addition to the aforementioned reaction preventing us from obtaining long cycle lifetimes, it was also difficult to discern whether Li^+ was incorporated into the body of $TiSi_2$; a competing explanation of the observed capacity

* Address correspondence to dunwei.wang@bc.edu.

Received for review June 20, 2012 and accepted August 23, 2012.

Published online August 23, 2012
10.1021/nn302734j

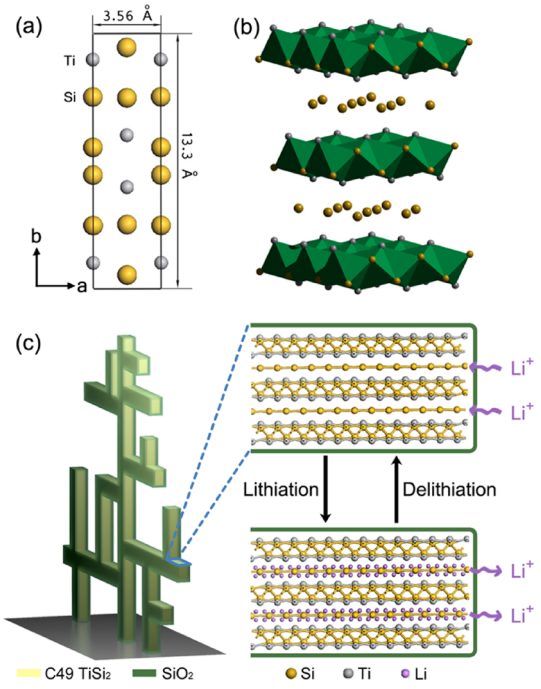

Figure 1. Schematic illustration of the C49 $TiSi_2$ crystal structure. (a) Side view of the unit cell along the [001] direction. (b) Perspective view of a polyhedron representation of the structure, in which the Si-only layer is shown as discrete atoms. (c) C49 $TiSi_2$ is stabilized by the nanonet morphology (left panel). The oxide coating is depicted as a green overlayer. The cartoons on the right show how Li^+ is incorporated into the Si-only layers.

would be that it comes from surface reactions. Addressing these issues should help us understand the detailed lithation mechanism. By forming a thin oxide coating on the surface of $TiSi_2$ nanonets, we solved the stability issue and were able to determine that Li^+ reacts with Si in the body of $TiSi_2$. Specific capacities close to 800 mA h g^{-1} were measured (705 mA h g^{-1} at the 200th cycle), and more than 80% of the original capacity was retained after 500 cycles of repeated lithiation and delithiation. Nevertheless, it is important to note that the results reported here are fundamentally different from our previous reports where we used $TiSi_2$ nanonets as a charge collector to improve the performance of Si nanoparticles,[19,20] as the present article focuses on understanding the intrinsic properties of $TiSi_2$.

RESULTS AND DISCUSSIONS

The $TiSi_2$ nanonets were obtained *via* the reaction between $TiCl_4$ and SiH_4 in a H_2-rich environment. A moderate growth temperature of 675 °C and a short growth time of 12 min yield a dense deposition; the average areal density of the synthesis was approximately 100 μg cm^{-2}. The oxide overlayer was formed by exposing as-synthesized $TiSi_2$ nanonets to ambient air at 350 °C and allowing them to cool to room temperature naturally. A TEM micrograph in the inset of Figure 2 demonstrates that a 4 nm oxide coating, amorphous in nature, was obtained. Other oxidation conditions, including different temperatures, durations, or a combination of the two, were also studied, and it was found that the reported conditions produced the best results. As will be discussed in more detail later, oxide coatings achieved *via* other methods such as atomic layer deposition serve the purpose of stabilizing $TiSi_2$ almost as well.

The resulting materials were tested using a two-electrode coin cell for charge/discharge characterizations or a three-electrode electrochemical cell for impedance studies. The typical charge/discharge behaviors are plotted in Figure 3a, b. A significant portion of the electrons that passed through the electrode during the first cycle were consumed in irreversible reactions, as evidenced by the disparity between the charge (lithiation; capacity: 3045 mA h g^{-1}) and discharge (delithiation; capacity: 943 mA h g^{-1}) curves. Similar behaviors have been frequently observed in other systems, although the exact nature of the irreversible processes remains unclear at this stage.[21] The disparity between charge and discharge curves disappeared after the first five cycles. Figure 3b shows the stability of oxide-coated $TiSi_2$ between the sixth and ninth cycles at a rate of 2000 mA g^{-1}, where the charge and discharge curves from each cycle overlap. Consistent with the plots, the calculated Coulombic efficiencies were greater than 98%. Note that due to the limited data sampling capability at the relatively fast charge/discharge rate of 2000 mA g^{-1} exhibited by the battery analyzer (BTS-5 V1 mA, Neware, China) utilized in the cycling tests, the reported Coulombic efficiencies may be systematically underestimated.

The stability of oxide-stabilized $TiSi_2$ nanonets can be better observed in the capacity *versus* cycle plots (Figure 3c), where the charge/discharge tests were extended to 500 cycles. For this group of data, the first five cycles were carried out at a rate of 200 mA g^{-1}; this rate was increased by 10-fold for subsequent cycles. To avoid crowding the plots, we only show one data point every five cycles. The capacity decreased from 744 mA h g^{-1} (at the 26th cycle) to 606 mA h g^{-1} (at the 500th cycle), corresponding to an overall capacity decay of 18.8%, or 0.04% per cycle. Again we note that the calculated Coulombic efficiency of greater than 98% was lower than the expected 99.96%, presumably due to system errors intrinsic to our instrumentation.

The rate performance of $TiSi_2$ is noteworthy. For a measured capacity of 744 mA h g^{-1} at a rate of 2000 mA g^{-1}, a charge or discharge process takes *ca.* 22 min. This rate performance is enabled by the good electrical conductivity of $TiSi_2$, *ca.* 10^5 S cm^{-1}. Because $TiSi_2$ nanonets were directly grown on conductive charge collectors, no binders were added to the system. The gaps between the beams of the $TiSi_2$ nanonets, typically larger than 50 nm, are expected to enable fast electrolyte diffusion as well. If we define

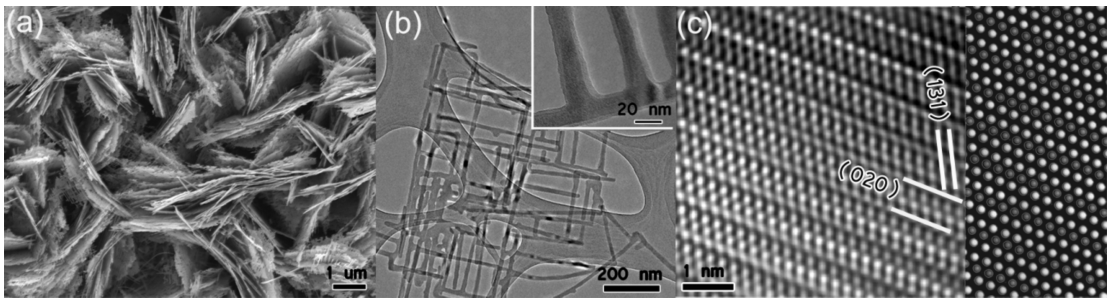

Figure 2. Microstructures of oxide-coated $TiSi_2$ nanonets. (a) Scanning electron micrograph showing the high purity of the nanonets. (b) Low-magnification transmission electron micrograph (TEM) revealing the two-dimensional connectivity of a nanonet. Inset: The oxide layer is clearly visible in the magnified view. (c) High-resolution TEM viewed along the {020} plane. The experimental data (left) match the simulated data (right), confirming the layered structure of C49 $TiSi_2$.

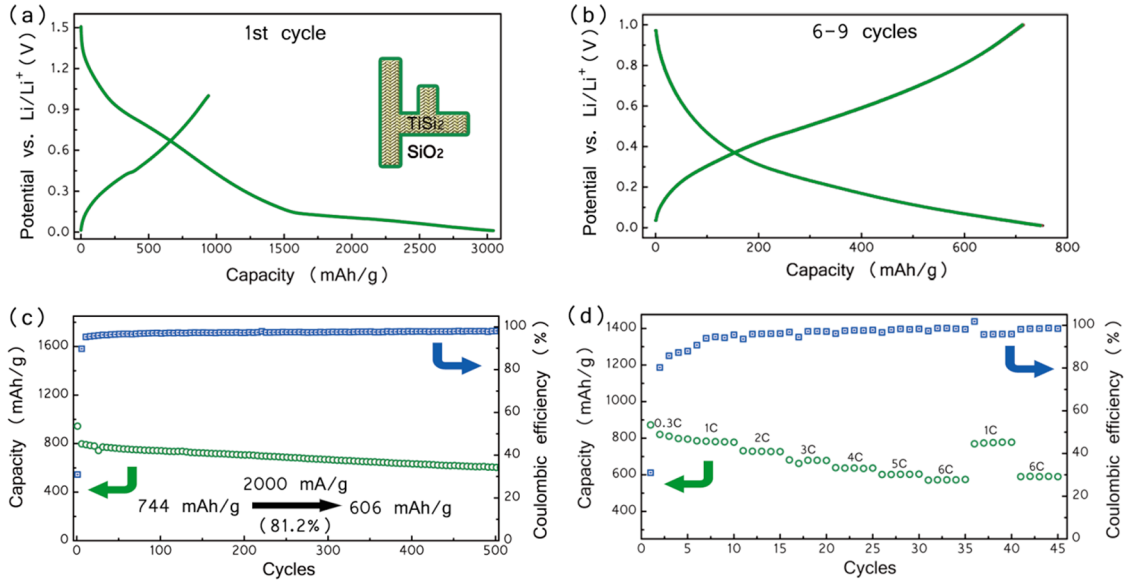

Figure 3. Electrochemical properties of oxide-stabilized $TiSi_2$ nanonets. (a) Charge/discharge characteristics of the first cycle. Rate: 200 mA g^{-1}; potential range: 1.5 to 0.01 V. (b) Charge/discharge curves from cycles 6 to 9 overlapping each other. Rate: 2000 mA g^{-1}; potential range: 1.0 to 0.01 V. (c) Retention of charge capacity and Coulombic efficiency at a rate of 2000 mA g^{-1}. Potential range: 1.0 to0.01 V. (d) Rate-dependent specific capacities. 1C is equivalent to 1029 mA g^{-1}. Potential range: 1.0 to 0.01 V.

1C as 1029 mA g^{-1}, Figure 3d plots how the capacity changed as the charge rates were varied between 0.3C and 6C. At 6C (6174 mA g^{-1}), the measured capacity was 574 mA h g^{-1}, corresponding to 74% of the value at 0.3C. Remarkably, more than 99.9% of the initial capacity was recovered when the cell was again measured at 1C.

The 1C value of 1029 mA g^{-1} was obtained by using the schematic structure shown in Figure 1c and assuming that only the Si layer contributes to the capacity. We also assumed each Si atom can host 4 Li^+, leading to a lithiated formula of Li_4TiSi_2 and, hence, a specific capacity of 1029 mA h g^{-1}. Of course, this coarse approximation lacks a theoretical basis and, as such, should be used only as a general reference. Notwithstanding the primitive estimation, this value is close to the measured specific capacities of 943 mA h g^{-1} at a charge rate of 200 mA g^{-1}.

We reiterate that the oxide coating on $TiSi_2$ is indispensable to the performance of the $TiSi_2$ anode. The capacity of $TiSi_2$ without the addition of an intentional oxide layer faded at a rate more than double that of an oxide-coated sample (Supporting Information, Figure S1 and Figure S2). The effect of an oxide coating has been discussed by other authors as well.[22−27] Some believe an oxide overlayer, when sufficiently thin, is permeable to ions (Li^+) but blocks electrons. The oxide layer in essence acts as a desired solid−electrolyte interface (SEI) or serves to facilitate SEI formation.[22] Others have proposed that oxides, SiO_2 in particular, may participate in the charge/discharge processes by reacting with Li^+ to form Li_xO and SiO_x, where $x < 2$.[28−30] In order to understand the nature of the improved performance imparted by an oxide coating, we carried out electrochemical impedance spectroscopy (EIS) measurements. The data for oxide-stabilized $TiSi_2$ in fully lithiated and delithiated forms are shown in Figure 4, and they should be compared to our previous work where EIS measurements of

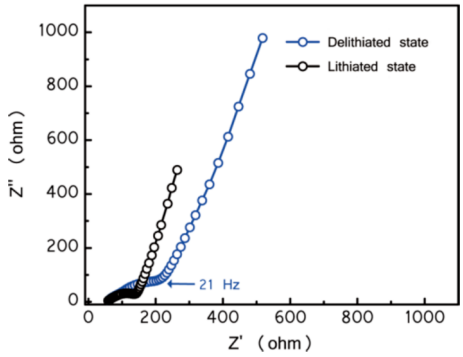

Figure 4. Electrochemical impedance *spectra* (in the form of Nyquist plots) of oxide-stabilized $TiSi_2$ nanonets. The sample was first fully lithiated to 0.01 V at 100 mA g^{-1}, and the system was permitted to reach equilibrium for 2 h before impedance data were taken. The frequency was varied between 50 kHz and 1 Hz, with an ac amplitude of 10 mV. Then the sample was discharged to 1 V at 100 mA g^{-1}, and impedance data were collected under the same conditions.

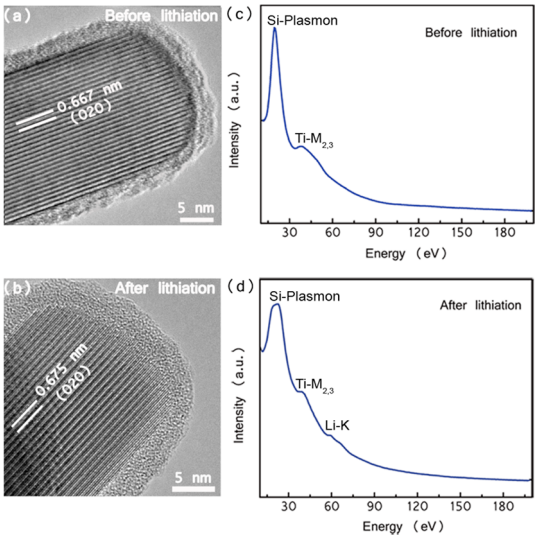

Figure 5. High-resolution TEM images of $TiSi_2$ before (a) and after (b) lithiation. (c and d) Electron energy loss spectroscopy of a $TiSi_2$ nanonet before (c) and after (d) lithiation.

oxide-free $TiSi_2$ were reported.[18] A fundamental difference is observed in the impedance after delithiation. For $TiSi_2$ without oxide, a drastic increase of impedance typically accompanied the delithation process; this change is attributed to changes in the SEI layer induced by lithiation and delithiation reactions.[21,31] Such an impedance change was largely absent in the oxide-stabilized $TiSi_2$ (Figure 4). This result implies that the oxide overlayer indeed alters the nature of the SEI layer. Additionally, the oxide coating acts as a mechanical screen to prevent the exfoliation of layered $TiSi_2$ during lithiation,[23,27,32] which would otherwise lead to an eventual mechanical breakdown of the electrode material. Taken as a whole, the improved SEI and the mechanical protection conferred by an oxide coating enable significantly enhanced cyclability of $TiSi_2$. In addition, by fitting the lithiated data, the charge transfer resistance was found to be only *ca.* 100 Ω, indicating the good charge conduction of the oxide-coated $TiSi_2$ (Supporting Information, Figure S3). While it is clear that adding an oxide layer to the system is beneficial to the stability of the anode, it is not clear whether the conferred stability is solely due to properties of the oxide or due to the possible modification of the SEI layer. Therefore, we do not intend to downplay the important role of the SEI layer.

Next we present evidence to support that Li^+ indeed inserts into the Si-only layer in $TiSi_2$. Because there is no known reaction between Ti and Li, it is safe to conclude that the observed capacity results from reactions between Si and Li^+. Comparing the lattice spacing of the $TiSi_2$ {020} planes before and after lithiation, we observed an increase from 0.667 to 0.675 nm, corresponding to a 1.2% change, and no measurable difference was observed along other crystal planes (Supporting Information, Figure S5). This small but non-negligible change indicates the insertion of Li^+ into the {020} planes, where Si-only layers reside. This hypothesis is supported by the electron energy loss spectroscopy result, which confirms the existence of Li ions in the lithiated sample (Figure 5d). In contrast, no Li signal was detected from the as-grown sample (Figure 5c). Benefitting from the small volume change upon Li^+ insertion and extraction, the layered-structure $TiSi_2$ exhibits better cycling stability than other Si-based alloys. In addition, the nanonet morphology and crystalline nature are well preserved after 100 cycles (Supporting Information, Figure S4).

Ideally, powder X-ray diffraction (XRD) patterns taken before lithiation and at various stages of charge and discharge would be useful in the task of elucidating the lithiation mechanism of $TiSi_2$. However, in this situation, specific limitations preclude the use of powder XRD data. On the basis of the observed *d*-spacing change presented in Figure 5, the shift in the (020) peak position would be 0.16°; this shift is based on the calculated values of 13.27° and 13.11° 2Θ (CuKα). In addition to the small peak shift, the (020) peak is not present is XRD diffraction patterns collected from as-grown $TiSi_2$ nanonets.[33] The broadening of the diffraction peak due to the small size of the nets would also complicate matters. Finally, the (060) peak could possibly be used, but it is partially eclipsed by the presence of the (131) peak.[33]

CONCLUSION

As the performance of electrochemical devices is intimately connected to the properties of their components, particularly those of the electrodes, the discovery of new compounds or new mechanisms is of great value to the advancement of energy storage technology. It is within this context that we believe our results are significant. The $TiSi_2$ nanonets, which are of the C49 crystal structure, represent a rare example of

a layered, nongraphite anode compound. This study was enabled by our strategy to stabilize layered $TiSi_2$ nanonets using an easy-to-implement oxide coating. The stabilized material survives up to 500 cycles of lithiation and delithation, making practical applications as electrodes for lithium-ion batteries possible. The stabilization also allowed us to perform detailed structural studies to confirm that Li ions are indeed reversibly inserted and extracted from the Si-only layer in $TiSi_2$ nanonets. This simple structure opens a doorway to significantly improved energy storage devices in terms of cyclability and power rate.

EXPERIMENTAL SECTION

$TiSi_2$ Synthesis. $TiSi_2$ nanonets were synthesized by chemical vapor deposition. Briefly, 50 sccm (standard cubic centimeters per minute) SiH_4 (10% in He), 2.5 sccm $TiCl_4$ (Sigma-Aldrich, 98%), and 100 sccm H_2 (Airgas) were delivered into a heated reactor in tandem. By keeping the reactor at 675 °C and 5 Torr for 12 min, we collected highly dense $TiSi_2$ nanonets on a piece of Pt-coated Ti foil (Sigma). The supplies of precursors were then cut off, and the reactor was cooled to room temperature with H_2 protection. The sample was then immediately transferred into an Ar-filled glovebox (O_2 < 2 ppm; Vacuum Atmosphere Co.) for coin-cell or electrochemical cell fabrications.

$TiSi_2/SiO_2$ Synthesis. The $TiSi_2$ nanonets with SiO_2 coatings were produced in the same fashion as those above, except that the reactor was opened to air at an elevated temperature (350 °C). A layer of SiO_2 was thermally formed during the cooling process.

$TiSi_2/Al_2O_3$ Synthesis. After growth, the $TiSi_2$ nanonets were transferred into the atomic layer deposition chamber immediately. Trimethylaluminum (TMA) (Sigma) and water were kept at room temperature and used as the Al and O precursors, respectively. The chamber was maintained at 200 °C during growth. The pulse time and purge time were 15 ms and 10 s for both TMA and water, respectively.

Coin Cell Fabrication. The as-synthesized samples were cut into 0.5 × 0.5 cm^2 pieces and assembled into CR2032-type coin cells with Li foils (Sigma-Aldrich; 0.38 mm) in a glovebox by a hydraulic crimping machine (MTI). $LiPF_6$ (1.0 M) in 1:1 wt/wt ethylene carbonate and diethyl carbonate (Novolyte Technologies) was used as electrolyte. Two CR2500 membranes (Celgard) were employed as a separator between the two electrodes.

Electrochemical Tests. After assembly, the coin cells were kept in a home-built box at a constant temperature of 30 °C. The cycling stability was characterized by a 16-channel battery analyzer (Neware, China; current range: 1 μA−1A).

The electrochemical impedance measurements were conducted using a CHI 600C potentiostat/galvanostat in an electrochemical cell. Two Li foils were used as both counter and reference electrodes, respectively. After fully lithiating or delithiating the materials at a slow charging/discharging rate (100 mA g^{-1}), we allowed the electrochemical cell to equilibrate for 2 h before collecting impedance data. The frequency was set between 50 kHz and 0.1 Hz, with 10 mV ac amplitude. All simulations were performed using ZsimpWin.

Structure Characterization. To obtain the structural information of the nanonets after testing, coin cells were opened in a glovebox and the tested electrodes were soaked in dimethoxyethane (Sigma; anhydrous; 99.5%) for 24 h to remove any electrolyte. The solvent was refreshed every 4 h. The morphology was characterized by a scanning electron microscope (SEM, model JSM 6340) and a transmission electron microscope (TEM, model JEOL 2010 F).

Electron Energy Loss Spectroscopy (EELS). EELS measurements were conducted for both unlithiated and lithiated samples. The measurements were conducted on a JEM-2010F TEM equipped with a parallel detection EELS spectrometer.

Conflict of Interest: The authors declare no competing financial interest.

Acknowledgment. The work is supported by Boston College and in part by MassCEC through a catalyst award. We thank D. Jiang and S. Boettcher for the insightful discussions.

Supporting Information Available: Comparison of cycling performances of $TiSi_2$ with and without SiO_2 overlayer; cycling performance of $TiSi_2$ nanonets with 1 nm Al_2O_3; electrochemical impedance spectroscopy measurement; morphology of $TiSi_2/SiO_2$ after 100 cycles; TEM of fully lithiated $TiSi_2$; SEM images of as-grown and lithiated $TiSi_2/SiO_2$ nanonets; oxide coating thickness and uniformity; method for the determination of the quantity of nanonets on a sample; high-resolution TEM image of the $TiSi_2/SiO_2$ interface. This material is available free of charge *via* the Internet at http://pubs.acs.org.

REFERENCES AND NOTES

1. Kazunori, O. Lithium-Ion Rechargeable Batteries with $LiCoO_2$ and Carbon Electrodes: The $LiCoO_2$/C System. *Solid State Ionics* **1994**, *69*, 212–221.
2. Tarascon, J. M.; Armand, M. Issues and Challenges Facing Rechargeable Lithium Batteries. *Nature* **2001**, *414*, 359–367.
3. Armand, M.; Tarascon, J. M. Building Better Batteries. *Nature* **2008**, *451*, 652–657.
4. Kim, H.; Han, B.; Choo, J.; Cho, J. Three-Dimensional Porous Silicon Particles for Use in High-Performance Lithium Secondary Batteries. *Angew. Chem., Int. Ed.* **2008**, *47*, 10151–10154.
5. Hu, Y.-S.; Demir-Cakan, R.; Titirici, M.-M.; Müller, J.-O.; Schlögl, R.; Antonietti, M.; Maier, J. Superior Storage Performance of a Si@SiO_x/C Nanocomposite as Anode Material for Lithium-Ion Batteries. *Angew. Chem., Int. Ed.* **2008**, *47*, 1645–1649.
6. Chan, C. K.; Peng, H.; Liu, G.; McIlwrath, K.; Zhang, X. F.; Huggins, R. A.; Cui, Y. High-Performance Lithium Battery Anodes Using Silicon Nanowires. *Nat. Nanotechnol.* **2008**, *3*, 31–35.
7. Kasavajjula, U.; Wang, C.; Appleby, A. J. Nano- and Bulk-Silicon-Based Insertion Anodes for Lithium-Ion Secondary Cells. *J. Power Sources* **2007**, *163*, 1003–1039.
8. Wolfenstine, J. $CaSi_2$ as an Anode for Lithium-Ion Batteries. *J. Power Sources* **2003**, *124*, 241–245.
9. Liu, W.-R.; Wu, N.-L.; Shieh, D.-T.; Wu, H.-C.; Yang, M.-H.; Korepp, C.; Besenhard, J. O.; Winter, M. Synthesis and Characterization of Nanoporous NiSi-Si Composite Anode for Lithium-Ion Batteries. *J. Electrochem. Soc.* **2007**, *154*, A97–A102.
10. Roberts, G. A.; Cairns, E. J.; Reimer, J. A. Magnesium Silicide as a Negative Electrode Material for Lithium-Ion Batteries. *J. Power Sources* **2002**, *110*, 424–429.
11. Deng, D.; Lee, J. Y. Reversible Storage of Lithium in a Rambutan-Like Tin−Carbon Electrode. *Angew. Chem., Int. Ed.* **2009**, *48*, 1660–1663.
12. Yu, Y.; Gu, L.; Wang, C.; Dhanabalan, A.; van Aken, P. A.; Maier, J. Encapsulation of Sn@Carbon Nanoparticles in Bamboo-Like Hollow Carbon Nanofibers as an Anode Material in Lithium-Based Batteries. *Angew. Chem., Int. Ed.* **2009**, *48*, 6485–6489.
13. Park, M.-S.; Wang, G.-X.; Kang, Y.-M.; Wexler, D.; Dou, S.-X.; Liu, H.-K. Preparation and Electrochemical Properties of SnO_2 Nanowires for Application in Lithium-Ion Batteries. *Angew. Chem., Int. Ed.* **2007**, *46*, 750–753.
14. Paek, S.-M.; Yoo, E.; Honma, I. Enhanced Cyclic Performance and Lithium Storage Capacity of SnO_2/Graphene Nanoporous Electrodes with Three-Dimensionally Delaminated Flexible Structure. *Nano Lett.* **2008**, *9*, 72–75.

15. Beyers, R.; Sinclair, R. Metastable Phase Formation in Titanium-Silicon Thin Films. *J. Appl. Phys.* **1985**, *57*, 5240–5245.
16. Netz, A.; Huggins, R.; Weppner, W. Investigations of a Number of Alternative Negative Electrode Materials for Use in Lithium Cells. *Ionics* **2001**, *7*, 433–439.
17. Zhou, S.; Liu, X.; Lin, Y.; Wang, D. Spontaneous Growth of Highly Conductive Two-Dimensional Single-Crystalline $TiSi_2$ Nanonets. *Angew. Chem., Int. Ed.* **2008**, *47*, 7681–7684.
18. Zhou, S.; Wang, D. Unique Lithiation and Delithiation Processes of Nanostructured Metal Silicides. *ACS Nano* **2010**, *4*, 7014–7020.
19. Zhou, S.; Liu, X. H.; Wang, D. W. Si/$TiSi_2$ Hetero-Nanostructures as High Capacity Anode Material for Li Ion Batteries. *Nano Lett.* **2010**, *10*, 860–863.
20. Xie, J.; Yang, X.; Zhou, S.; Wang, D. Comparing One- and Two-Dimensional Heteronanostructures as Silicon-Based Lithium Ion Battery Anode Materials. *ACS Nano* **2011**, *5*, 9225–9231.
21. Chan, C. K.; Ruffo, R.; Hong, S. S.; Cui, Y. Surface Chemistry and Morphology of the Solid Electrolyte Interphase on Silicon Nanowire Lithium-Ion Battery Anodes. *J. Power Sources* **2009**, *189*, 1132–1140.
22. Xiao, X.; Lu, P.; Ahn, D. Ultrathin Multifunctional Oxide Coatings for Lithium Ion Batteries. *Adv. Mater.* **2011**, *23*, 3911–3915.
23. Cho, J.; Kim, Y. J.; Kim, T.-J.; Park, B. Zero-Strain Intercalation Cathode for Rechargeable Li-Ion Cell. *Angew. Chem., Int. Ed.* **2001**, *40*, 3367–3369.
24. Kim, J. S.; Johnson, C. S.; Vaughey, J. T.; Hackney, S. A.; Walz, K. A.; Zeltner, W. A.; Anderson, M. A.; Thackeray, M. M. The Electrochemical Stability of Spinel Electrodes Coated with ZrO_2, Al_2O_3, and SiO_2 from Colloidal Suspensions. *J. Electrochem. Soc.* **2004**, *151*, A1755–A1761.
25. Fan, Y.; Wang, J.; Tang, Z.; He, W.; Zhang, J. Effects of the Nanostructured SiO_2 Coating on the Performance of $LiNi_{0.5}Mn_{1.5}O_4$ Cathode Materials for High-Voltage Li-Ion Batteries. *Electrochim. Acta* **2007**, *52*, 3870–3875.
26. Fu, L. J.; Liu, H.; Li, C.; Wu, Y. P.; Rahm, E.; Holze, R.; Wu, H. Q. Surface Modifications of Electrode Materials for Lithium Ion Batteries. *Solid State Sci.* **2006**, *8*, 113–128.
27. Zhang, T.; Gao, J.; Zhang, H. P.; Yang, L. C.; Wu, Y. P.; Wu, H. Q. Preparation and Electrochemical Properties of Core-Shell Si/SiO Nanocomposite as Anode Material for Lithium Ion Batteries. *Electrochem. Commun.* **2007**, *9*, 886–890.
28. Sun, Q.; Zhang, B.; Fu, Z.-W. Lithium Electrochemistry of SiO_2 Thin Film Electrode for Lithium-Ion Batteries. *Appl. Surf. Sci.* **2008**, *254*, 3774–3779.
29. Miyachi, M.; Yamamoto, H.; Kawai, H.; Ohta, T.; Shirakata, M. Analysis of SiO Anodes for Lithium-Ion Batteries. *J. Electrochem. Soc.* **2005**, *152*, A2089–A2091.
30. Abel, P. R.; Lin, Y.-M.; Celio, H.; Heller, A.; Mullins, C. B. Improving the Stability of Nanostructured Silicon Thin Film Lithium-Ion Battery Anodes through Their Controlled Oxidation. *ACS Nano* **2012**, *6*, 2506–2516.
31. Ruffo, R.; Hong, S. S.; Chan, C. K.; Huggins, R. A.; Cui, Y. Impedance Analysis of Silicon Nanowire Lithium Ion Battery Anodes. *J. Phys. Chem. C* **2009**, *113*, 11390–11398.
32. Wu, H.; Chan, G.; Choi, J. W.; Ryu, I.; Yao, Y.; McDowell, M. T.; Lee, S. W.; Jackson, A.; Yang, Y.; Hu, L.; *et al*. Stable Cycling of Double-Walled Silicon Nanotube Battery Anodes through Solid-Electrolyte Interphase Control. *Nat. Nanotechnol.* **2012**, *7*, 310–315.
33. Zhou, S.; Liu, X.; Lin, Y.; Wang, D. Rational Synthesis and Structural Characterizations of Complex $TiSi_2$ Nanostructures. *Chem. Mater.* **2009**, *21*, 1023–1027.